Spectrally Wide-Band Terahertz Wave Modulator Based on Optically Tuned Graphene

Peter Weis,[†] Juan L. Garcia-Pomar,[†,‡,§] Michael Höh,[†,‡] Benjamin Reinhard,[†] Alexander Brodyanski,[⊥] and Marco Rahm[†,‡,*]

[†]Department of Physics and Research Center OPTIMAS, University of Kaiserslautern, Erwin-Schroedinger-Strasse, 67663 Kaiserslautern, Germany, [‡]Fraunhofer Institute for Physical Measurement Techniques IPM, Heidenhofstrasse 8, 79110 Freiburg, Germany, and [⊥]Institut für Oberflächen- und Schichtanalytik IFOS GmbH and Research Center OPTIMAS, Trippstadter Straße 120, 67663 Kaiserslautern, Germany. [§]Present address: Department of Condensed Matter Physics, University of Zaragoza, 50009 Zaragoza, Spain.

ABSTRACT New applications in the realms of terahertz (THz) technology require versatile adaptive optics and powerful modulation techniques. Semiconductors have proven to provide fast all-optical terahertz wave modulation over a wide frequency band. We show that the attenuation and modulation depth in optically driven silicon modulators can be significantly enhanced by deposition of graphene on silicon (GOS). We observed a wide-band tunability of the THz transmission in a frequency range from 0.2 to 2 THz and a maximum modulation depth of 99%. The maximum difference between the transmission through silicon and GOS is $\Delta t = 0.18$ at a low photodoping power of 40 mW. At higher modulation power, the enhancement decreased due to charge carrier saturation. We developed a semianalytical band structure model of the graphene–silicon interface to describe the observed attenuation and modulation depth in GOS.

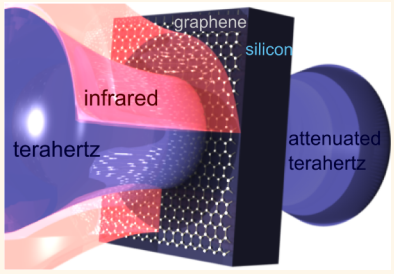

KEYWORDS: tunable metamaterials · graphene · terahertz waves · wide-band terahertz wave modulation · broadband modulation · photodoping of graphene · enhanced modulation depth

Terahertz (THz) research became a spotlight of scientific interest driven by a vast amount of new applications in the realms of security technology,[1,2] quality control in the pharmaceutic and plastics industry,[3,4] astronomy, and sensing.[5–7] Most of these applications benefit from the observation that a large number of materials are transparent for THz waves, which allows one to detect the properties of inclusions or materials behind dielectric obstacles such as plastics, textiles, paper, cardboard, and much more. However, the aforementioned applications also demand high standards for the employed THz technology and necessitate the development of efficient THz sources and detectors. Moreover, the various application fields define stringent requirements for high-performance optical components such as waveplates, lenses, and modulators, which are readily available for the optical, infrared, and microwave regions of the electromagnetic spectrum but not necessarily for the THz frequency regime. In this context, metamaterials have recently proven to offer a promising approach for the implementation of birefringent, nonlinear, and tunable optical designer media.[8–10]

Another material that has been drawn into the focus of attention is graphene. Since its discovery in 2004, a whole range of experiments evidenced its exceptional physical properties.[11] The observation of massless charge carriers in graphene has implied intriguing consequences. For example, it was possible to verify principles of relativistic quantum mechanics and more specifically the quantum Hall effect in graphene.[12,13] In the last years, it became evident that graphene can play a significant role with respect to its application in optics. Specifically in the THz region and far-infrared graphene seems to provide suitable properties that can be exploited for the design and implementation of one atomic layer thin transformation optical devices.[14–16] Moreover, continuous layers of graphene as well as periodically structured graphene support confined surface plasmons with very small wavelengths.[17–23] It is not surprising that metamaterials can highly benefit from the extraordinary electronic properties of graphene when it is embedded in metamaterial structures.[24–26] Recently, Liu *et al.* developed a modulator for the optical region based on graphene that was integrated in a waveguide.[27] For THz waves, Ju *et al.* successfully realized tunable metamaterials by means of integrated structured graphene, whose

* Address correspondence to mrahm@physik.uni-kl.de.

Received for review July 27, 2012 and accepted September 19, 2012.

Published online September 19, 2012
10.1021/nn303392s

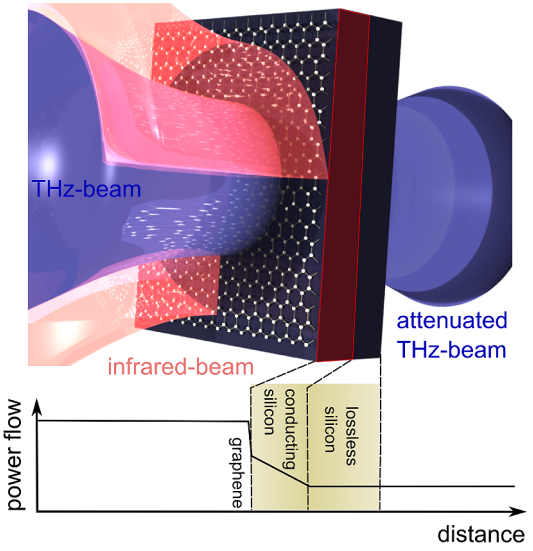

Figure 1. Illustration of the experiment (not to scale). The top part depicts a schematic view of the graphene on silicon sample, the spatial configuration of modulation, and THz beam as well as the layered structure used for the model. The bottom graph illustrates the spatial dependence of the THz beam power along the sample as calculated from the model when the modulation beam is switched on.

conductivity could be modulated by a gate voltage. In the same context, Sensale-Rodriguez *et al.* proposed and demonstrated voltage-controlled beam modulation in graphene on semiconductor heterostructures.[28,29]

Here, we show that graphene on top of silicon (GOS) is highly suitable for efficient optically driven amplitude modulation of terahertz waves. In comparison with pure silicon, we observed strongly enhanced modulation in GOS over a wide frequency range from 0.2 THz up to 2 THz at identical power levels of the photodoping beam. At a photodoping power of 40 mW we measured a decreased amplitude transmission t of the GOS averaged in the range from 0.2 to 1.0 THz of $t = 0.21$. Compared to the transmission in pure silicon ($t = 0.39$) at the same power level, the transmission was almost halved due to the one atomic graphene layer (see Figure 3). The modulation depth $[M = (E_0 - E_P)/E_0]$, which is defined by the difference between the transmitted field amplitude E_0 without photodoping and the transmitted field amplitude E_P under illumination normalized to E_0, is $M = 0.69$ for GOS and only $M = 0.45$ for pure silicon at the same photodoping power of 40 mW. In order to explain the enhancement of the modulation depth that is induced by graphene, we developed a semianalytical band structure model that allowed us to calculate, predict, and explain the physical mechanism of the expected attenuation of terahertz waves in photodoped silicon and GOS. The hybrid material system GOS has potential applications for THz modulators and tunable optical components. By proper spatial shaping of the optical photodoping beam this approach can be potentially used for the generation of appropriate conductivity

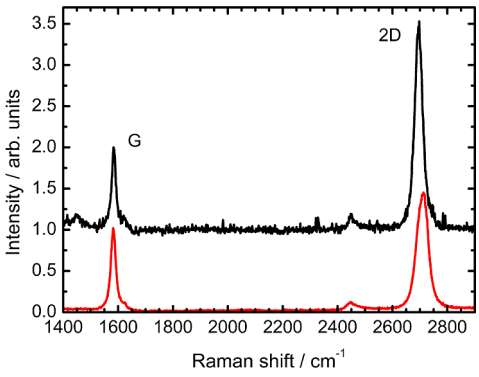

Figure 2. Raman spectra of the GOS sample at different locations on the surface. The measurements were performed with a laser of wavelength $\lambda = 488$ nm and a spot size on the sample of ~2.5 mm. The spectra are normalized to the G-band maximum.

patterns in GOS to implement transformation-optical devices as suggested in ref 14.

RESULTS AND DISCUSSION

Experiment. We analyzed the GOS, whose fabrication is described in detail in the Methods section, *via* Raman spectroscopy to evaluate the quality of the obtained graphene layer. By this means, we evidenced the presence of prevalent regions with monolayered graphene on the silicon substrate, but also identified small isles with two or more layers of graphene and graphite as well as void regions without carbon material. To distinguish between the carbon modifications, we used two characteristic spectrum features well known from literature: (i) the height ratio between the G and 2D bands, (ii) the frequency of the 2D band.[30] Figure 2 depicts some measured Raman spectra. We assigned the Raman spectrum shown by the black curve to an area with single-layer graphene, since the 2D band is positioned at ~2695 cm^{-1} and is more than twice the height of the corresponding G band. The red curve can be assigned to bilayer graphene, the 2D band is shifted to ~2709 cm^{-1}, and the G and 2D bands exhibit similar heights. Another characteristic feature of bilayer graphene that is shown by the red curve is the broadened and asymmetric 2D band, since it is composed of four bands.[30] Because each of the identified graphene regions is considerably smaller than the THz beam focus, the transmission of THz waves through the GOS modulator is defined by the electronic properties of a mixture of graphene layers with varying quality. Although it is expected that the observed enhancement of the modulation depth in photodoped GOS depends on the quality of the graphene layer, we could still observe a significant effect.

We measured the spectral transmission of the GOS modulator by standard THz-time domain spectroscopy. Therefore, we focused the THz wave to a spot diameter of 2 mm and placed the GOS modulator in the focus. For photodoping of the GOS we used a

pulsed laser (wavelength $\lambda = 780$ nm, pulse duration $\tau \approx 100$ fs). We aligned the laser beam to overlap with the THz beam. We mounted the GOS in a metallic sample holder with a circular aperture. The diameter of the aperture was $d \approx 2$ mm, corresponding to the full width at half-maximum of the THz beam. By this means, we assured exclusive detection of the transmission through the overlapping regions of the THz and the modulation beam. Despite the transient operation of the modulating laser, only the time-averaged power transfer to the GOS sample contributed to the free carrier generation and thus the magnitude of the modulation depth. This follows from the long lifetime of charge carriers ($\tau \geq 1\ \mu$s) in weakly doped silicon, which is significantly longer than the pulse repetition time ($\tau_r = 12.5$ ns) of the employed laser. For verification we determined the dynamical behavior of the photodoping by changing the temporal offset between THz and modulation pulse at the location of the GOS sample. As expected, the photodoping was independent of the time delay. For additional confirmation we replaced the pulsed laser by a continuous wave laser with similar power at a wavelength of $\lambda = 405$ nm and obtained comparable modulation depths (not shown in this publication), which moreover indicates the wavelength independence of the photodoping.

Figure 3 shows the amplitude spectra of the transmitted electric THz field through the silicon and GOS samples, respectively. The spectra are normalized to a reference spectrum without sample. Without photodoping, silicon provides a high transmission, up to $t \approx 1$. The frequency-dependent modulation in the transmission amplitude is caused by interference of repeatedly reflected waves at the silicon surfaces. Upon photodoping electron–hole pairs are induced within a volume that is defined by the penetration depth of the modulation beam and the illuminated area. The increase of the conductivity causes a broadband attenuation of the transmitted THz wave, as shown in Figure 3 for a photodoping power of 40 mW. Comparing GOS with silicon, we expected and experimentally observed a decrease of the transmission amplitude of about 2.3% for GOS without photodoping due to interband transitions in graphene.[31,32] Upon photodoping of GOS, the transmission of the THz wave decreases over a wide frequency range from 0.2 to 2 THz. Compared to silicon the THz beam attenuation is significantly enhanced at equivalent power levels of the photodoping. This is clearly shown in Figure 3, where the THz wave transmission through GOS at a photodoping power of 40 mW is about half that for silicon.

A more detailed study revealed that GOS is especially advantageous to silicon with respect to the obtainable modulation depth at low photodoping levels. Figure 4a shows the dependence of the amplitude transmission t averaged over a frequency window from 0.2 to 1 THz on the power of the modulation beam P. At low power

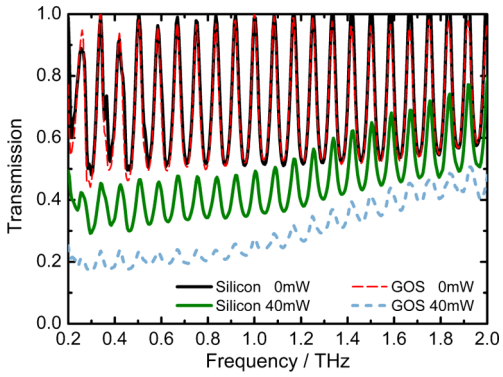

Figure 3. Transmission spectra of the silicon and GOS samples without illumination and with photodoping at a power of $P = 40$ mW.

levels the transmission through GOS is significantly lower than through silicon. At $P = 40$ mW, the difference between the transmission through GOS and silicon is maximal at a value of $\Delta t = 0.18$. For increasing power levels exceeding 40 mW the photodoping in both GOS and silicon starts to saturate and the amplitude transmission of GOS converges to the values of silicon. At a modulation power of 500 mW the transmission through GOS and silicon is comparable. This behavior is also mirrored by the modulation depth. Figure 4b depicts the modulation depth M in dependence on the modulation beam power once again averaged over the frequency region from 0.2 to 1 THz. Similar to the observed attenuation displayed in Figure 4a, a maximum enhancement of the modulation depth for GOS can be observed at low photodoping power levels, up to 40 mW, while the difference in the modulation depth between GOS and silicon decreases for increasing power due to saturation effects. As a result, GOS is an advantageous material system that can be used as a highly efficient all-optical modulator for THz waves in a wide frequency range from 0.2 to 2 THz at low optical photodoping power. In order to explain the enhancement of the modulation depth, we developed a semianalytical model, which is described in the next section.

Model. In the following we describe a semianalytical model to calculate the spectral transmission and the modulation depth of THz radiation through GOS. We modeled the GOS as a multistack system consisting of a graphene film on top of a silicon layer with photodoping-dependent conductivity followed by a lossless silicon substrate. This scheme is depicted in Figure 1. The modulation beam is incident from the graphene side and is partially reflected from the top and bottom surfaces of the graphene film. A small fraction of the modulation beam is absorbed in graphene, which is characterized by a uniform absorption spectrum in the infrared and optical frequency regime.[32,33] The magnitude of the absorption associated with interband transitions amounts to $\pi\alpha \approx 2.3\%$, where α is the fine structure constant. The nonabsorbed transmitted

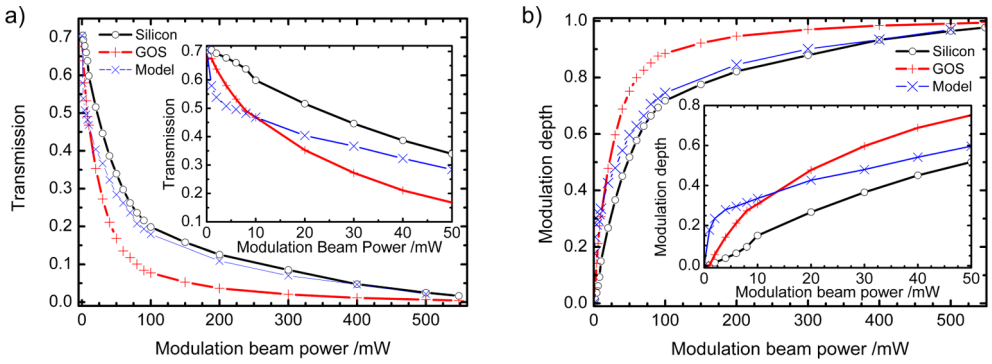

Figure 4. (a) THz amplitude transmission and (b) modulation depth, averaged over a frequency window from 0.2 to 1 THz with dependence on the modulation power as measured for the bare silicon (circles) and the GOS (crosses). The corresponding amplitude transmission and the modulation depth obtained from the semianalytical model are shown for comparison (crosses, dashed) in (a) and (b). The insets in (a) and (b) show an excerpt of the amplitude transmission and the modulation depth for modulation power levels in the range from $P = 0$ mW to $P = 50$ mW.

fraction of the beam penetrates the silicon substrate, and most of the energy is completely absorbed within the penetration length defined by the absorption coefficient. In other words, the major fraction of free charge carriers is generated within a volume defined by the beam width and the penetration length of the modulation beam in silicon. In good approximation, it is justified to subdivide the silicon substrate into a lossy layer with a thickness defined by the penetration length and a lossless silicon stack that influences only the phase of the transmitted THz wave. The free charge carriers induce a change of the electric conductivity, which is inherently correlated with a decrease of the THz transmission through the material. The THz absorbance and reflectivity of silicon are dependent on the change of conductivity and increase with increasing modulation beam power. Comparing the amount of absorbed energy of the modulation beam in graphene and silicon, one notices that the number of generated electron–hole pairs in graphene is negligible compared with the number of free carriers originating from the silicon substrate. For compensation of the charge gradient the free carriers diffuse from the silicon substrate into the graphene layer until a steady state is reached. When arriving in graphene, these charge carriers experience a tremendously higher mobility than their silicon counterparts and hence contribute to a stronger change of conductivity than observed in silicon.[11,28,34] As discussed and experimentally evidenced above, this results in an enhancement of the attenuation of THz waves in GOS in comparison with the transmission through pure silicon. The enhancement effect becomes even more dominant when the thickness of the semiconductor substrate is reduced. Keeping this in mind, it should be possible to devise advanced ultrathin THz modulators by alternating graphene–silicon multilayer structures.

In order to describe reflection and absorption in the multistack, it was necessary to determine the band structure scheme of the system that is shown in Figure 5. The electronic behavior of silicon can be described by

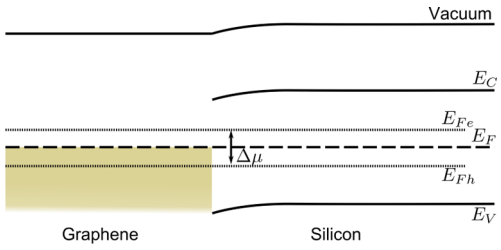

Figure 5. Band scheme of the GOS material. E_c denotes the conduction band energy, E_v the energy of the valence band, E_F the Fermi level energy, E_{Fe} and E_{Fh} the quasi Fermi energies for electrons and holes, and $\Delta\mu = E_{Fe} - E_{Fh}$ the quasi-Fermi level splitting.

the quasi-Fermi levels of electrons and holes in the quasi-thermal equilibrium. In analogy to a doped semiconductor, the conductivity σ in silicon can be expressed in terms of the separation energy ($\Delta\mu = E_{Fe} - E_{Fh}$) of the quasi-Fermi levels (E_{Fe} and E_{Fh}) for electrons and holes by

$$\sigma = e(\mu_n N_c + \mu_p N_v) e^{-E_g/2k_BT} e^{\Delta\mu/2k_BT} \quad (1)$$

Herein, e is the elementary charge, μ_n and μ_p are the charge mobilities of electrons and holes, N_c/N_v are the density of states in the conduction/valence band, and $E_g = E_c - E_v$ is the bandgap of the semiconductor. Since more electron–hole pairs are excited in silicon than in graphene, a gradient of the charge density and hence of the quasi-Fermi level splitting is induced at the graphene–silicon interface. As stated by Ryzhii *et al.*,[35] the change of the quasi-Fermi level splitting in photodoped graphene can be calculated by $\Delta\mu = 12\alpha[(\hbar v_F)^2/k_BT][\tau_r I/\hbar\Omega]$. With the characteristic recombination time $\tau_r = 1$ ns, the modulation laser frequency Ω corresponding to the wavelength of $\lambda = 780$ nm, and the maximum intensity $I =$ 500 mW/($\pi \cdot 1$ mm^2) used in our experiments the quasi-Fermi level energy separation amounts to $\Delta\mu \approx 5$ meV, which is equivalent to the values reported in ref 36. This value is negligible compared to the splitting of the quasi-Fermi levels in silicon ($\Delta\mu \approx 0.3$ eV) obtained from eq 1 assuming a moderate conductivity, $\sigma = 100$ Sm. In consequence, the difference in the separation energy

of the quasi-Fermi levels in silicon and graphene is compensated by diffusion currents $J_n = \mu_n n \nabla E_{F_e}$ for electrons and $J_p = \mu_p p \nabla E_{F_h}$ for holes until the quasi-Fermi level splitting of both silicon and graphene are balanced. In the diffusion process a small number of carrier charges transported to the graphene sheet is already sufficient to strongly influence the assimilation of the quasi-Fermi level splitting in graphene and silicon. We therefore obtain the band scheme as illustrated in Figure 5. Consequently, we can calculate the quasi-Fermi level splitting in graphene by eq 1. Furthermore, the conductivity of the graphene layer at frequency ω and temperature T can be obtained from[35,37,38]

$$\sigma_{inter} = e^2/(4\hbar)\tanh\left(\frac{\hbar\omega - 2\Delta\mu}{4k_BT}\right) \quad (2)$$

$$\sigma_{intra} = \frac{2e^2k_BT\tau \ln(1 + e^{\Delta\mu/k_BT})}{\pi\hbar^2(1 + \omega^2\tau^2)} \quad (3)$$

where k_B is the Boltzmann constant and $\hbar$ is the Planck constant. The recombination time τ of graphene depends on the graphene-layer quality. To determine the separation of the quasi-Fermi levels ($\Delta\mu$), we numerically calculated the spectral transmission of silicon, applying the aforementioned two-layer approximation of silicon as schematically illustrated in Figure 1. In a further step we added an infinitesimally thin layer of graphene with the calculated values σ_{inter} and σ_{intra} on top of the silicon and numerically calculated the spectral transmission through the GOS material. In this simulation, we chose the recombination time $\tau = 55$ fs as a free parameter to fit the numerical results to the experimental data at a modulation power of 10 mW and kept this value constant for all other photodoping power levels. Details about the numerical calculations and used parameters can be found in the Methods section.

The numerically obtained spectral transmission and the corresponding modulation depth are displayed in Figure 4a and b. With respect to the spectral transmission of THz waves through the GOS, the numerical results agree well with the experimental data up to a modulation beam power of 30 mW. For increasing beam power the agreement worsens and the transmission approaches the values of pure silicon, as can be seen in Figure 4a. The reason for the deviation at higher pump power levels is rooted in the fact that we did not account for heating of the sample by the laser as well as saturation processes in silicon. Both effects evoke an increase of the penetration depth, which was not quantified in the semianalytic model. Furthermore, the relations between the graphene conductivity and the Fermi levels as described by eq 2 and eq 3 are based on the conical band structure of graphene, which is strictly applicable only for small energies. Thus, this model strongly underestimates the number of states that can be occupied *via* intraband transitions at high modulation intensities. This results in inaccuracies of the graphene conductivity. Despite the known deficiencies of the idealized model, the derived band scheme and the corresponding calculations strongly support the physical understanding of the processes occurring at the interface between graphene and silicon and their implications for the electromagnetic properties of GOS.

CONCLUSION

We experimentally demonstrated that graphene on silicon can be used as an efficient, spectrally wide-band all-optical modulator for terahertz waves. Our experiments evidence that photodoped GOS provides a significantly enhanced attenuation and modulation depth in comparison with a pure silicon-based modulator. We measured a maximal modulation depth of 99% for the GOS sample and amplitude modulation in a wide frequency band from 0.2 to 2 THz. In comparison with pure silicon, a maximum difference of $\Delta t = 0.18$ of the amplitude transmission was observed in GOS at a photodoping power of 40 mW. In order to understand the enhancement effect, we developed a semianalytical model that describes the band structure of the graphene–silicon interface and numerically calculated the spectral transmission and the optically driven modulation depth of GOS. Since the modulation effect is mainly based on the excitation of free charge carriers near the graphene–silicon interface, GOS has the potential to serve as an ultrathin terahertz wave modulator. In a future perspective, spatially shaped optical modulation beams could be applied to obtain spatially dependent terahertz wave modulation. This might pave the way toward new transformation-optical devices as suggested in ref 14. Continuous wave (CW) lasers are readily available and can provide sufficient power in the required wavelength range to efficiently drive the amplitude modulation in GOS with adequate modulation depth. Hence, CW lasers are a proper choice for a practical implementation of all-optical GOS terahertz wave modulators. Furthermore, the enhanced THz absorption within a small volume could be used for the implementation of temperature-sensitive terahertz detectors.

METHODS

Fabrication of Graphene on Silicon. For the fabrication of GOS we used commercially available graphene, which was grown on a copper foil by chemical vapor deposition.[39] The obtained graphene films are continuous and predominantly single-layered, as specified by the manufacturer. The silicon substrate had a thickness of $d = 533$ μm. To ensure high THz transmission, the silicon was only weakly phosphor-doped and therefore possessed a low resistivity of $R \geq 3000$ Ωcm. For the transfer of graphene to the silicon substrate we adhered the graphene

on the copper sample to a thermal release tape. After etching off the copper, we applied the tape to the polished surface of a silicon substrate and removed it afterward by heating it to the release temperature.[40,41]

Numerical Methods. For all simulations we used the frequency domain solver of CST Microwave Studio. We chose the thickness of the first silicon layer to match the penetration depth of the modulation laser, which was about 5 μm. The second silicon layer was lossless and had a thickness of 528 μm. That way, the thicknesses of both silicon layers added up to the total thickness of the silicon wafer used in the experiment. By this means, we determined the silicon conductivity with dependence on the modulation beam power and calculated the quasi-level splitting ($\Delta\mu$) in silicon by use of eq 1 and the literature values $\mu_n = 1400\ cm^2/(V\ s)$, $\mu_p = 450\ cm^2/(V\ s)$, $N_c = 3.22 \times 10^{19}\ cm^{-3}$, $N_v = 1.83 \times 10^{19}\ cm^{-3}$, and $E_g = 1.12$ eV for silicon at room temperature. On the basis of the quasi-Fermi splitting ($\Delta\mu$) in silicon we derived the interband conductivity (σ_{inter}) and the intraband conductivity (σ_{intra}) of the graphene sheet with dependence on the modulation beam power by eq 2 and eq 3.

Conflict of Interest: The authors declare no competing financial interest.

Acknowledgment. We thank the Nano Structuring Center at the University of Kaiserslautern for their support in the sample fabrication. P.W. acknowledges financial support by the OPTIMAS Carl-Zeiss-Ph.D. program. G.-P. acknowledges financial support from Consolider Nanolight (CSD2007-00046).

REFERENCES AND NOTES

1. Hoshina, H.; Sasaki, Y.; Hayashi, A.; Otani, C.; Kawase, K. Noninvasive Mail Inspection System with Terahertz Radiation. *Appl. Spectrosc.* **2009**, *63*, 81–86.
2. Melinger, J. S.; Harsha, S. S.; Laman, N.; Grischkowsky, D. Temperature Dependent Characterization of Terahertz Vibrations of Explosives and Related Threat Materials. *Opt. Express* **2010**, *18*, 27238–27250.
3. Ho, L.; Müller, R.; Römer, M.; Gordon, K.; Heinämäki, J.; Kleinebudde, P.; Pepper, M.; Rades, T.; Shen, Y.; Strachan, C.; *et al*. Analysis of Sustained-Release Tablet Film Coats Using Terahertz Pulsed Imaging. *Pharm. Technol. Eur.* **2007**, *119*, 253–261.
4. Piesiewicz, R.; Jansen, C.; Wietzke, S.; Mittleman, D.; Koch, M.; Kürner, T. Properties of Building and Plastic Materials in the THz Range. *Int. J. Infrared Millimeter Waves* **2007**, *28*, 363–371.
5. Yoshida, S.; Suizu, K.; Kato, E.; Nakagomi, Y.; Ogawa, Y.; Kawase, K. THz Imaging Techniques for Nondestructive Inspections. *J. Mol. Spectrosc.* **2009**, *256*, 146–151.
6. Shibuya, T.; Suzuki, T.; Suizu, K.; Kawase, K. Non-destructive Characterization of Soot in Exhaust Filters Using Millimeter-Wave Imaging. *J. Infrared, Millimeter, Terahertz Waves* **2011**, *32*, 716–721.
7. Theuer, M.; Harsha, S. S.; Molter, D.; Torosyan, G.; Beigang, R. Terahertz Time-Domain Spectroscopy of Gases, Liquids, and Solids. *ChemPhysChem* **2011**, *12*, 2695–2705.
8. Chen, H.-T.; O'Hara, J. F.; Azad, A. K.; Taylor, A. J.; Averitt, R. D.; Shrekenhamer, D. B.; Padilla, W. J. Experimental Demonstration of Frequency-Agile Terahertz Metamaterials. *Nat. Photonics* **2008**, *2*, 295–298.
9. Weis, P.; Paul, O.; Imhof, C.; Beigang, R.; Rahm, M. Strongly Birefringent Metamaterials as Negative Index Terahertz Wave Plates. *Appl. Phys. Lett.* **2009**, *95*, 171104.
10. Neu, J.; Krolla, B.; Paul, O.; Reinhard, B.; Beigang, R.; Rahm, M. Metamaterial-Based Gradient Index Lens with Strong Focusing in the THz Frequency Range. *Opt. Express* **2010**, *18*, 27748–27757.
11. Novoselov, K. S.; Geim, A. K.; Morozov, S. V.; Jiang, D.; Zhang, Y.; Dubonos, S. V.; Grigorieva, I. V.; Firsov, A. A. Electric Field Effect in Atomically Thin Carbon Films. *Science* **2004**, *306*, 666–669.
12. Novoselov, K. S.; Geim, A. K.; Morozov, S. V.; Jiang, D.; Katsnelson, M. I.; Grigorieva, I. V.; Dubonos, S. V.; Firsov, A. A. Two-Dimensional Gas of Massless Dirac Fermions in Graphene. *Nature* **2005**, *438*, 197–200.
13. Aaron Bostwick, T. O.; Seyller, T.; Horn, K.; Rotenberg, E. Quasiparticle Dynamics in Graphene. *Nat. Mater.* **2007**, *3*, 36–40.
14. Vakil, A.; Engheta, N. Transformation Optics Using Graphene. *Science* **2011**, *332*, 1291–1294.
15. Chen, P.-Y.; Alù, A. Atomically Thin Surface Cloak Using Graphene Monolayers. *ACS Nano* **2011**, *5*, 5855–5863.
16. Sun, Y.; Edwards, B.; Alù, A.; Engheta, N. Experimental Realization of Optical Lumped Nanocircuits at Infrared Wavelengths. *Nat. Mater.* **2012**, *11*, 208–2012.
17. Rana, F. Graphene Terahertz Plasmon Oscillators. *IEEE Trans. Nanotechnol.* **2008**, *7*, 91–99.
18. Popov, V.; Bagaeva, T. Y.; Otsuji, T.; Ryzhii, V. Oblique Terahertz Plasmons in Graphene Nanoribbon Arrays. *Phys. Rev. B* **2010**, *81*, 073404.
19. Nikitin, A. Y.; Guinea, F.; Garcia-Vidal, F. J.; Martin-Moreno, L. Fields Radiated by a Nanoemitter in a Graphene Sheet. *Phys. Rev. B* **2011**, *84*, 195446.
20. Nikitin, A. Y.; Guinea, F.; Garcia-Vidal, F. J.; Martin-Moreno, L. Edge and Waveguide Terahertz Surface Plasmon Modes in Graphene Microribbons. *Phys. Rev. B* **2011**, *84*, 161407.
21. Nikitin, A. Y.; Guinea, F.; Garcia-Vidal, F. J.; Martin-Moreno, L. Surface Plasmon Enhanced Absorption and Suppressed Transmission in Periodic Arrays of Graphene Ribbons. *Phys. Rev. B* **2012**, *85*, 081405.
22. Chen, J.; Badioli, M.; Alonso-González, P.; Thongrattanasiri, S.; Huth, F.; Osmond, J.; Spasenovic, M.; Centeno, A.; Pesquera, A.; Godignon, P.; *et al*. Optical Nano-Imaging of Gate-Tunable Graphene Plasmons. *Nature* **2012**, *487*, 77–81.
23. Fei, Z.; Rodin, A. S.; Andreev, G. O.; Bao, W.; McLeod, A. S.; Wagner, M; Zhang, L. M.; Zhao, Z.; Thiemens, M.; Dominguez, G.; *et al*. Gate-Tuning of Graphene Plasmons Revealed by Infrared Nano-Imaging. *Nature* **2012**, DOI: 10.1038/nature11253.
24. Papasimakis, N.; Luo, Z.; Shen, Z. X.; Angelis, F. D.; Fabrizio, E. D.; Nikolaenko, A. E.; Zheludev, N. I. Graphene in a Photonic Metamaterial. *Opt. Express* **2010**, *18*, 8353–8359.
25. Lee, S. H.; Choi, M.; Kim, T.-T.; Lee, S.; Liu, M.; Yin, X.; Choi, H. K.; Lee, S. S.; Choi, C.-G.; Choi, S.-Y.; *et al*. Switching Teraherz Waves with Gate-Controlled Active Graphene Metamaterials. *arXiv:1203.0743*, **2012**.
26. Zou, Y.; Tassin, P.; Koschny, T.; Soukoulis, C. M. Interaction Between Graphene and Metamaterials: Split Rings *vs.* Wire Pairs. *Opt. Express* **2012**, *20*, 12198–12204.
27. Liu, M.; Yin, X.; Ulin-Avila, E.; Geng, B.; Zentgraf, T.; Ju, L.; Wang, F.; Zhang, X. A Graphene-Based Broadband Optical Modulator. *Nature* **2011**, *474*, 64–67.
28. Sensale-Rodriguez, B.; Fang, T.; Yan, R.; Kelly, M. M.; Jena, D.; Liu, L.; Xing, H. G. Unique Prospects for Graphene-Based Terahertz Modulators. *Appl. Phys. Lett.* **2011**, *99*, 113104.
29. Sensale-Rodriguez, B.; Yan, R.; Kelly, M. M.; Fang, T.; Tahy, K.; Hwang, W. S.; Jena, D.; Liu, L.; Xing, H. G. Broadband Graphene Terahertz Modulators Enabled by Intraband Transitions. *Nat. Commun.* **2012**, *3*, article no. 780.
30. Ferrari, A. C.; Meyer, J. C.; Scardaci, V.; Casiraghi, C.; Lazzeri, M.; Mauri, F.; Piscanec, S.; Jiang, D.; Novoselov, K. S.; Roth, S.; *et al*. Raman Spectrum of Graphene and Graphene Layers. *Phys. Rev. Lett.* **2006**, *97*, 187401.
31. Peres, N. M. R. Colloquium: The Transport Properties of Graphene: An Introduction. *Rev. Mod. Phys.* **2010**, *82*, 2673–2700.
32. Tomaino, J. L.; Jameson, A. D.; Kevek, J. W.; Paul, M. J.; van der Zande, A. M.; Barton, R. A.; McEuen, P. L.; Minot, E. D.; Lee, Y.-S. Terahertz Imaging and Spectroscopy of Large-Area Single-Layer Graphene. *Opt. Express* **2011**, *19*, 141–146.
33. Kravets, V. G.; Grigorenko, A. N.; Nair, R. R.; Blake, P.; Anissimova, S.; Novoselov, K. S.; Geim, A. K. Spectroscopic Ellipsometry of Graphene and an Exciton-Shifted van Hove Peak in Absorption. *Phys. Rev. B* **2010**, *81*, 155413.
34. Morozov, S.; Novoselov, K. S.; Katsnelson, M. I.; Schedin, F.; Elias, D. C.; Jaszczak, J. A.; Geim, A. K. Giant Intrinsic Carrier

Mobilities in Graphene and Its Bilayer. *Phys. Rev. Lett.* **2008**, *100*, 016602.
35. Ryzhii, V.; Ryzhii, M.; Otsuji, T. Negative Dynamic Conductivity of Graphene with Optical Pumping. *J. Appl. Phys.* **2007**, *101*, 083114.
36. Boubanga-Tombet, S.; Chan, S.; Watanabe, T.; Satou, A.; Ryzhii, V.; Otsuji, T. Ultrafast Carrier Dynamics and Terahertz Emission in Optically Pumped Graphene at Room Temperature. *Phys. Rev. B* **2012**, *85*, 035443.
37. Ryzhii, V.; Ryzhii, M.; Satou, A.; Otsuji, T.; Dubinov, A. A.; Aleshkin, V. Y. Feasibility of Terahertz Lasing in Optically Pumped Epitaxial Multiple Graphene Layer Structures. *J. Appl. Phys.* **2009**, *106*, 084507.
38. Ryzhii, V.; Dubinov, A. A.; Otsuji, T.; Mitin, V.; Shur, M. S. Terahertz Lasers Based on Optically Pumped Multiple Graphene Structures with Slot-Line and DielectricWaveguides. *J. Appl. Phys.* **2010**, *107*, 054505.
39. Li, X.; Cai, W.; An, J.; Kim, S.; Nah, J.; Yang, D.; Piner, R.; Velamakanni, A.; Jung, I.; Tutuc, E.; *et al*. Large-Area Synthesis of High-Quality and Uniform Graphene Films on Copper Foils. *Science* **2009**, *324*, 1312–1314.
40. Bae, S.; Kim, H.; Lee, Y.; Xu, X.; Park, J.-S.; Zheng, Y.; Balakrishnan, J.; Lei, T.; Kim, H. R.; Song, Y. I.; *et al*. Roll-To-Roll Production of 30-Inch Graphene Films for Transparent Electrodes. *Nat. Nanotechnol.* **2010**, *5*, 574–578.
41. Geim, A. K.; Novoselov, K. S. The Rise of Graphene. *Nat. Mater.* **2007**, *6*, 183–191.